JCTC Journal of Chemical Theory and Computation

pubs.acs.org/JCTC Article

Density Functional Computations of Vibrational Circular Dichroism Spectra beyond the Born–Oppenheimer Approximation

Josef Tomeček and Petr Bouř*

Cite This: *J. Chem. Theory Comput.* 2020, 16, 2627–2634

Read Online

ACCESS | Metrics & More | Article Recommendations | SI Supporting Information

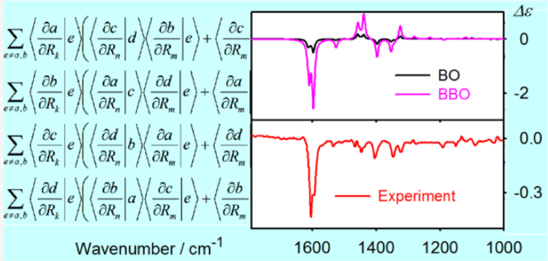

ABSTRACT: Transition-metal complexes provide rich features in vibrational circular dichroism (VCD) spectra, including significant intensity enhancements, and become thus useful in structural and functional studies of molecules. Quite often, however, the vibrational spectral bands are mixed with the electronic ones, and interpretation of such experiments is difficult. In the present study, we elaborate on the theory needed to calculate the VCD intensities beyond the Born–Oppenheimer (BO) approximation. Within a perturbation approach, the coupling between the electronic and vibrational states is estimated using the harmonic approximation and simplified wave functions obtainable from common density functional theory (DFT) computations. Explicit expressions, including Slater determinants and derivatives of molecular orbitals, are given. On a model diamine complex, the implementation is tested and factors affecting spectral intensities and frequencies are investigated. For two larger molecules, the results are in a qualitative agreement with previous experimental data. Typically, the electronic–vibrational interaction Hamiltonian coupling elements are rather small (~0 to 10 cm^{-1}), which provides negligible contributions to vibrational frequencies and absorption intensities. However, significant changes in VCD spectra are induced due to the large transition magnetic dipole moment associated with the d–d metal transitions. The possibility to model the spectra beyond the BO limit opens the way to further applications of chiral spectroscopy and transition-metal complexes.

1. INTRODUCTION

As pointed out already by Born and Oppenheimer (BO),[1] electronic and nuclear motions in molecules are rather independent, and coupling of the electronic and vibrational states is limited.[2] Still, it can occur and be used in many spectroscopic studies, such as those including low-lying electronic states.[3] The vibrational circular dichroism (VCD) technique seems to be particularly suitable to monitor such situations. VCD measures differential absorption of left and right circularly polarized light and is more sensitive to molecular structure than unpolarized absorption (IR).[4,5] It is also more sensitive to the interference of the electronic and vibrational transitions.[6] Sometimes, the "beyond BO" (BBO) effects even provide enhancement of the VCD signal. This boosts the sensitivity of the technique and significantly widens its application range.

Typical systems where BBO effects were observed contain metals with d–d or f–f transitions. The splitting of degenerate energy levels in the metal due to the coordinated ligands provides low-lying electronic states that can resonate with the vibrational ones. Many examples of such VCD experiments are given in ref 3. Quite often, they include transition-metal complexes of Co(II, III) or Ni(II). The metal ion is sometimes thought of as the smallest imaginable probe reflecting the environment. Also, various chiral ligands were explored, such as sparteine,[6,7] bisureate,[8] and a range of salicyldiminate anions.[9,10] Apart from the low-lying electronic states, these complexes often have in common the frequent presence of unpaired electrons. For example, Domingos et al. demonstrated that complexes of paramagnetic Co^{2+} with amino acid and oligopeptides exhibited the VCD enhancement, while the diamagnetic Co^{3+} close-shell counterparts did not.[11]

Experimental VCD signs, absolute and relative intensities may differ from the theory.[6,9−11] Although not all "atypical" spectral features can be attributed to the BBO coupling, disagreement between experimental and theoretical VCD patterns computed in the standard way may indicate this effect.

Strictly speaking, computation of the atomic axial tensor (AAT) needed for VCD intensities in some sense always goes beyond the BO concept. The standard procedure, used also here, is based on Stephens' magnetic field perturbation (MFP) theory and derivatives of electronic ground state BO wave function.[12] However, derivations of the MFP formulae or other computational approaches do take into account BBO effects.[12−14] In the present study, however, we focus on a different aspect, mixing of the vibrational and electronic states.

Received: January 23, 2020
Published: March 5, 2020

https://dx.doi.org/10.1021/acs.jctc.0c00081

Within a perturbation concept and the vibronic coupling theory, this mixing and its consequences for VCD modeling have been elaborated by Nafie.[3,15] Here, we follow a similar philosophy consisting of (1) the Herzberg−Teller expansion of the electronic wave function with respect to nuclear coordinates, (2) incorporation of the BBO interaction terms in molecular Hamiltonian, and (3) using the general expressions for the dipole and rotational strengths. Unlike in ref 3, we (1) explicitly investigate resultant terms (integrals) for a wave function based on the Slater determinants, (2) derive the needed integrals in the basis of atomic/molecular orbitals (MOs), and (3) estimate involved variables and final effects on the spectra for molecular examples. Such an implementation of the BBO treatment in quantum-chemical codes is not known to us. The combination of the Slater Kohn−Sham (KS) determinant wave function with perturbation expansions allows one to overcome the complexity of the general expressions, containing in principle multidimensional integrals. BBO corrections to VCD intensities can then be relatively easily implemented within the formalism of the density functional theory (DFT).[16]

Below, we briefly review the BO concept and introduce the necessary notation. In Sections 2.1 and 2.2, the BBO wave function in the BO basis is introduced within the usual quantum-chemical formalism.[3,17] In Section 2.3, the perturbation elements are expressed in a BO electronic wave function expanded to the second order with respect to nuclear coordinates and further elaborated for a wave function composed of singly excited DFT (KS) determinants in Section 2.4. Mathematical details are additionally provided in the Supporting Information (SI). In the rest of the theoretical section, the usual expressions for absorption and VCD intensities within the harmonic approximation are introduced.[3,18] Rather than using a perturbation approach from ref 3, the spectral intensities are estimated using full diagonalization of the BBO Hamiltonian expressed in the basis of BO wave functions, to avoid eventual problems with degenerate energy levels. The implementation, stability of the results with respect to basis set size, functional, etc. are discussed for a model diamine molecule. Finally, the predicted BBO effects in VCD spectra of two larger cobalt complexes are compared with previous experiments. It appears that the approach allows if not for accurate reproduction, then at least for a qualitative estimation of the BBO effects in VCD spectroscopy.

2. THEORY

2.1. Born−Oppenheimer Approximation.

The general molecular Hamiltonian can be written as

$$H(R, P, p, r) = H_e(R, p, r) + T_N \tag{1}$$

where R and P represent nuclear positions and momenta, respectively. Similarly, r and p stand for the electronic positions and momenta, $H_e(R, p, r) = T_e + V(R, r)$ is the electronic Hamiltonian, T_N/T_e is the nuclear/electronic kinetic energy, and $\hat{V}(R, r)$ is the Coulomb electron-nuclear potential.

Within the BO approximation,[1] the wave function is considered as a product of electronic $e_J(R, r)$ and vibrational $v_{jJ}(R)$ parts, $\psi_{jJ} = e_J(R, r)v_{jJ}(R)$. Capital letters are reserved for electronic states and small ones for vibrational ones; the J in ν_{jJ} means that the vibrational wave function depends on the electronic state as well. The wave functions obey so-called nuclear and electronic Schrödinger equations

$$\begin{aligned} H_e e_J(R, r) &= \varepsilon_J(R) e_J(R, r) \\ H_{NJ} v_{iJ}(R) &= \varepsilon_{iJ}(R) v_{iJ}(R) \end{aligned} \tag{2}$$

where $H_{NJ} = T_N + \varepsilon_J(R)$ is the nuclear (vibrational) Hamiltonian.

2.2. General Wave Function.

Functions ψ_{jJ}, however, do not obey the Schrödinger equation

$$H\Psi_e = E_e\Psi_e \tag{3}$$

where Ψ_e is the exact wave function. There are immense difficulties associated with the rigorous "ab initio" description of molecules beyond the BO approach.[19] However, for many practical computations, Ψ_e may be expanded into the BO basis

$$\Psi_e = \sum_{jJ} c_{jJ}^e \psi_{jJ} \tag{4}$$

and the remaining BBO "correction" is usually treated as a perturbation.[15] The Schrödinger eq 3 then adopts a matrix form, $\mathbf{Hc} = \mathbf{Ec}$, with Hamiltonian elements $H_{kK,jJ} = \langle\psi_{kK}|H|\psi_{jJ}\rangle$. The matrices $\mathbf{c}$ and $\mathbf{E}$ collect the expansion coefficients c_{kK}^e and energies E_e. From eqs 1 and 2, we get

$$\begin{aligned} H_{kK,jJ} &= \langle e_K(R, r)v_{kK}(R)|H_e + T_N|e_J(R, r)v_{jJ}(R)\rangle \\ &= \langle e_K(R, r)v_{kK}(R,)|H_e|e_J(R, r)v_{jJ}(R)\rangle \\ &\quad + \langle e_K(R, r)v_{kK}(R)|T_N|e_J(R, r)v_{jJ}(R)\rangle \\ &= \langle v_{kK}(R)|\varepsilon_J(R) + T_N|v_{jJ}(R)\rangle\langle e_K|e_J\rangle \\ &\quad + \langle v_{kK}(R)e_K(R, r)|[T_N, e_J(R, r)]|v_{jJ}(R)\rangle \end{aligned}$$

Therefore,

$$H_{kK,jJ} = \varepsilon_{jJ}\delta_{JK}\delta_{jk} + \langle v_{kK}|V_{KJ}|v_{jJ}\rangle \tag{5}$$

$$\begin{aligned} V_{KJ} &= \langle e_K|[T_N, e_J]\rangle \\ &= -\frac{\hbar^2}{2}\sum_n \frac{1}{M_n}\left\langle e_K \middle| \frac{\partial^2 e_J}{\partial R_n^{\,2}} \right\rangle \\ &\quad - i\hbar \sum_n \frac{1}{M_n}\left\langle e_K \middle| \frac{\partial e_J}{\partial R_n} \right\rangle P_n \end{aligned} \tag{6}$$

where the interaction elements $V_{KJ}(R, P)$ are responsible for the BBO (often referred to as nonadiabatic or non-BO) effects.[17]

2.3. Working Expressions.

For smaller deformations, we expand the electronic wave function e_J to the second order with respect to deviations of nuclei from their equilibrium positions, $\Delta R_n = R_n - R_{n0}$

$$e_J(\Delta R) = J + \sum_n J_n \Delta R_n + \frac{1}{2}\sum_{n,m} J_{nm}\Delta R_n \Delta R_m \tag{7}$$

For more compact notation, we defined $J = e_J(0)$, $J_n = \left.\frac{\partial e_J}{\partial R_n}\right|_0$, and $J_{nm} = \left.\frac{\partial^2 e_J}{\partial R_n \partial R_m}\right|_0$. This form can be used to express the integrals in eq 6, for example,

$\left\langle e_K \middle| \frac{\partial^2 e_J}{\partial R_n^2} \right\rangle = \langle K + \sum_n K_n \Delta R_n + \frac{1}{2} \sum_{n,m} K_{nm} \Delta R_n \Delta R_m | J_{nn} \rangle$, etc. After some algebra (cf. SI), we obtain

$$V_{KJ} \cong \nu_0 + \sum_m \nu_{R,m} \Delta R_m + \sum_m \nu_{P,m} P_m \tag{8}$$

where $\nu_0 = \sum_n \frac{\hbar^2 \langle K_n | J_n \rangle}{2M_n}$, $\nu_{R,m} = \sum_n \frac{\hbar^2}{2M_n} [\langle K_n | J_{nm} \rangle + \langle K_{nm} | J_n \rangle]$, and $\nu_{P,m} = -\frac{i\hbar}{M_m} \langle K | J_m \rangle$. Higher orders, up to the third power of the nuclear coordinates, can be found in Appendix I (SI).

2.4. Electronic Wave Function. The wave function is approximated by a sum of Slater determinants Δ_j, $e_J(0) = \sum_j C_j^J \Delta_j$, obtained from the time-dependent density functional theory (TDDFT).[20,21] The determinants contain only single excitations, which further facilitates the computation. In the past, this approximation of the wave function provided reasonably realistic molecular properties, such as magnetic circular dichroism spectra.[22] It leads to explicit expressions for V_{KJ} based and derivatives of the coefficients C_j^J and determinants Δ_j (cf. Appendices II and III, SI, for details). Similar approach suitable for multiconfiguration or configuration interaction (CI) procedures can be found elsewhere.[23]

Elaborating the terms in eq 8, we get

$$\begin{aligned} \nu_0 = {} & \sum_n \sum_k \frac{\hbar^2}{2M_n} \frac{\partial C_k^K}{\partial R_n} \frac{\partial C_k^J}{\partial R_n} \\ & + \sum_n \frac{\hbar^2}{2M_n} \sum_k \sum_j \left(\frac{\partial C_k^K}{\partial R_n} C_j^J - C_k^K \frac{\partial C_j^J}{\partial R_n} \right) \left\langle \Delta_k \middle| \frac{\partial \Delta_j}{\partial R_n} \right\rangle \\ & + \sum_n \frac{\hbar^2}{2M_n} \sum_k \sum_j C_k^K C_j^J \left\langle \frac{\partial \Delta_k}{\partial R_n} \middle| \frac{\partial \Delta_j}{\partial R_n} \right\rangle \\ \nu_{R,m} = {} & \frac{\hbar^2}{2M_m} \left[\sum_k \left(\frac{\partial C_k^K}{\partial R_m} \frac{\partial^2 C_k^J}{\partial R_m^2} + \frac{\partial^2 C_k^K}{\partial R_m^2} \frac{\partial C_k^J}{\partial R_m} \right) \right. \\ & + \sum_k \sum_j \left(\frac{\partial C_k^K}{\partial R_m} C_j^J + C_j^K \frac{\partial C_k^J}{\partial R_m} \right) \left\langle \Delta_k \middle| \frac{\partial^2 \Delta_j}{\partial R_m^2} \right\rangle \\ & + \sum_k \sum_j \left(\frac{\partial^2 C_k^K}{\partial R_m^2} C_j^J - C_k^K \frac{\partial^2 C_j^J}{\partial R_m^2} \right) \left\langle \Delta_k \middle| \frac{\partial \Delta_j}{\partial R_m} \right\rangle \\ & \left. + 2 \sum_k \sum_j \left(C_k^K \frac{\partial C_j^J}{\partial R_m} + \frac{\partial C_k^K}{\partial R_m} C_j^J \right) \left\langle \frac{\partial \Delta_k}{\partial R_m} \middle| \frac{\partial \Delta_j}{\partial R_m} \right\rangle \right] \\ \nu_{P,m} = {} & -\frac{i\hbar}{M_n} \left[\frac{1}{2} \sum_k \left(C_k^K \frac{\partial C_k^J}{\partial R_n} - \frac{\partial C_k^K}{\partial R_n} C_k^J \right) \right. \\ & \left. + \sum_k \sum_j C_k^K C_j^J \left\langle \Delta_k \middle| \frac{\partial \Delta_j}{\partial R_n} \right\rangle \right] \end{aligned} \tag{9}$$

As shown in the SI, the overlap integrals with the Slater determinants reduce to one-electron integrals of molecular orbitals or their derivatives. For example, $\left\langle \Delta_k \middle| \frac{\partial \Delta_k}{\partial R_n} \right\rangle = 0$ because of the normalization of the wave function ($\langle \Delta k | \Delta k \rangle = 1$), $\left\langle \Delta_j \middle| \frac{\partial \Delta_k}{\partial R_n} \right\rangle = \left\langle c \middle| \frac{\partial d}{\partial R_k} \right\rangle$ when Δ_k differs from Δ_j by single molecular orbital c replaced by d, etc. Of course, for the second derivatives and more complicated cases, the expression becomes more complex and automatic derivation and programming were used to avoid formal errors.

2.5. Vibrational Wave Function. We use the vertical approximation,[24] where the vibrational function is the same for all electronic states and equal to the harmonic oscillator wave function. Then, the matrix elements $\langle \nu_{kK} | V_{KJ} | \nu_{jJ} \rangle$ in eq 5 can be obtained analytically using the vibrational normal mode coordinates Q_N and the Cartesian—normal mode transformation matrix $\mathbf{S}$[25]

$$R_n = \sum_N S_{nN} Q_N \tag{10}$$

The **S**-matrix elements and harmonic vibrational frequencies (e.g., energies ε_{iJ} in eq 2) were thus computed using the usual diagonalization of the harmonic force field (second energy derivatives with respect to nuclear coordinates).[5]

2.6. Spectral Intensities. IR and circular dichroic spectral intensities for a transition i → f are proportional to the dipole and rotational strength, respectively, defined as[18]

$$D = \mathrm{Re} \sum_\alpha \langle \mathrm{i} | \mu_\alpha | \mathrm{f} \rangle \langle \mathrm{f} | \mu_\alpha | \mathrm{i} \rangle \tag{11}$$

$$R = \mathrm{Im} \sum_\alpha \langle \mathrm{i} | \mu_\alpha | \mathrm{f} \rangle \langle \mathrm{f} | m_\alpha | \mathrm{i} \rangle \tag{12}$$

where μ_α / m_α is the α-component of the electric/magnetic dipole moment. Using the wave functions from eq 4, the dipole moment matrix elements ($d = \mu_\alpha$ or m_α) become

$$\langle \mathrm{i} | d | \mathrm{f} \rangle = \sum_{kK} c_{kK}^{\mathrm{i}} c_{jJ}^{\mathrm{f}} \langle v_k | d_{KJ} | v_j \rangle \tag{13}$$

The electronic transition dipole matrix element $d_{KJ} = \langle K | d | J \rangle$ can be further expanded in the nuclear coordinates

$$d_{KJ} \cong d_{KJ}(0) + \sum_m \frac{\partial d_{KJ}}{\partial Q_m} Q_m + \sum_m \frac{\partial d_{KJ}}{\partial P_m} P_m \tag{14}$$

In the present implementation, the derivative terms in eq 14 were included only for $J = K$, and only transitions from the ground state ($K = 0$) were considered. Similarly, as for the **S**-matrix, the dipole derivatives in eq 14 were obtained from a quantum-chemical program as specified below.

3. DENSITY FUNCTIONAL THEORY COMPUTATIONS

A model diamine molecule was used to evaluate the magnitude and basic properties of the BBO calculus; the methodology was then applied to larger sparteine—Co and salicyl—Co complexes (Figure 1). For the two larger systems, previous experiments were available in refs 6, 10. The geometries were optimized by energy minimization, using the Gaussian program,[26] B3LYP functional,[16,27] and a standard 6-311+G** basis set as defaults. For the bigger salicyl—Co, the lowest-energy conformer (mol01 from ref 10, providing 92% of conformer populations) was considered only. Other functionals (B3PW91, CAM-B3LYP) and basis sets (6-31G*, 6-31G**, 6-311+G*, 6-311++G**, def2-TZVP, and LANL2DZ Co pseudopotential) were also explored in the case of the diamine (cf. Table S1 with electronic energies). In general, the functional and basis set variation did not lead to significantly different results. For

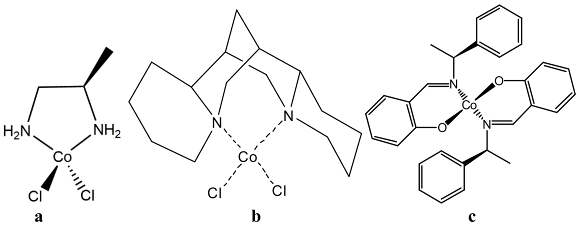

Figure 1. Model molecules: (a) diamine (R-1,2-diaminopropanedichlorocobalt(II)), (b) 6R,7S,9S,11S-(−)-sparteine.-CoCl$_2$ ("sparteine−Co"), and (c) bis[(S)-N-(1-phenylethyl) salicylal diminato] Δ-cobalt(II) ("salicyl−Co") complexes.

sparteine−Co, the molecular environment was mimicked by the conductor-like screening model (COSMO) with parameters for water,[28−30] which again did not bring qualitative changes. Multiplicity $M = 4$ was chosen for all molecules as it provided the smallest energy. Gaussian bands of 10 cm^{-1} bandwidths were used to plot the diamine spectra; for the other two molecules, further details are listed in Table S2 in the SI. Absorption (ε) and VCD ($\Delta\varepsilon$) are plotted in units of M^{-1}·cm^{-1}.

4. RESULTS AND DISCUSSION

4.1. Effect of the Spin.

Unlike most organic molecules, transition-metal complexes occur in various spin states, experimental determination of which can be quite challenging.[31] The multiplicity of the metal complexes can also significantly affect their vibrational spectra.[10] In an extreme case, the wrong spin determination can cause misinterpretation of the VCD data including the extent of the BBO effects. For the diamine, all combinations of tested functionals and basis sets (B3LYP and B3PW91; 6-31G**, 6-311+G**, and def2-TZVP) provided the lowest energy for multiplicity $M = 4$. For example, energies of states with $M = 2$ were by about 0.034 Hartree higher. The same result was obtained for sparteine−Co and salicyl−Co complexes, which is consistent with previous experiments, e.g., the absolute value of the total (orbital and spin) magnetic moment of sparteine−Co was determined as $\mu_{\text{eff}} = 4.12$ Bohr magnetons.[32]

The dependence of IR and VCD diamine spectra on the spin can be seen in Figure 2. The spectra for $M = 2$ and 4 are compared as calculated at the B3LYP/6-311+G** approximation level. Clearly, whereas IR intensities look nearly identical for both multiplicities, VCD spectra significantly differ not only in magnitude but also in signs of some peaks. As an extreme, the VCD intensity of the 1635 cm^{-1} band is enhanced about 20 times by the 2 → 4 multiplicity change. VCD thus also appears as a sensitive technique for spin determination.

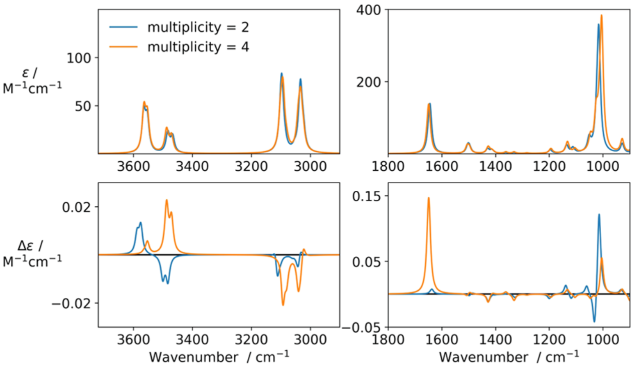

Figure 2. IR and VCD diamine spectra simulated for two multiplicities.

4.2. Orbital Derivatives.

The derivatives of molecular orbitals (MOs) with respect to nuclear coordinates are needed to evaluate the BBO potential matrix elements (eq 9, Appendices III and IV in the SI). The first and second derivatives were expressed in the basis of unperturbed MOs $\psi_i(0)$,

$$\frac{\partial \psi_a}{\partial R_n} = \sum_b \tilde{U}^a_{n,b}\psi_b(0)$$

$$\frac{\partial^2 \psi_a}{\partial R_n \partial R_n} = \sum_b \tilde{U}^a_{nn,b}\psi_b(0) \tag{15}$$

where the coefficients $\tilde{U}^a_{n,b}$ were obtained both from coupled-perturbed (CP) equations[33] and by numerical differentiation, using overlaps between equilibrium and perturbed orbitals. $\tilde{U}^a_{nn,b}$ we calculated by two-point differentiation only. The CP results are available in the Gaussian output via the IOp options.

The differentiation is more universal than the CP approach because it enables one to evaluate the first and second diagonal derivatives of the orbitals at the same time (eqs III.3 and III.4 in the SI). On the other hand, its accuracy is in principle dependent on the differentiation step size and some orbitals (in particular those with similar energies) may not change their shapes smoothly during the differentiation. For higher-energy orbitals, unrealistically strict criteria need to be applied for the self-consistent energy evaluation. Therefore, orbital rotations and phase corrections need to be applied while computing the derivatives numerically. This was done by unifying orbital phases at the distorted (perturbed) geometries with those at the equilibrium geometry. Typically, the overlap integral between the perturbed and equilibrium molecular orbital was close to 1 or −1 and ambiguities were rare. When they occurred, the perturbed orbitals were rotated to maximize their overlap with the equilibrium ones.

Occasionally, even the CP derivative coefficients obtained from Gaussian were not usable, typically for orbitals with nearly degenerate or high energies, probably because of the finite accuracy limits for the coupled-perturbed self-consistent computations.[34]

Because of these potential problems, we implemented both the numerical and analytical methods to compute the orbital derivatives, whereby comparing the results occasional errors could be corrected. In the final effect, however, both methods were found nearly equivalent. For example, the problematic high-energy orbitals do not much overlap with the lower-energy ones and inaccuracy in their derivatives has little effect on the observable quantities. The examples of typical correlations between the analytical and numerical derivatives are given in Figure 3a,b. The orbital derivatives exhibit larger variations across different functionals and basis sets (Figure 3c,f), although the core and frontier orbitals have a similar shape (Figure S1). Overall, the evaluation of the derivatives seems to be controllable and stable for a given approximation level.

4.3. Derivatives of the CI Coefficients.

In Figure 4, selected derivatives are calculated with the 0.005 and 0.02 Å differentiation steps. Apparently, also the estimation of the CI coefficient derivatives by the numerical differentiation seems to

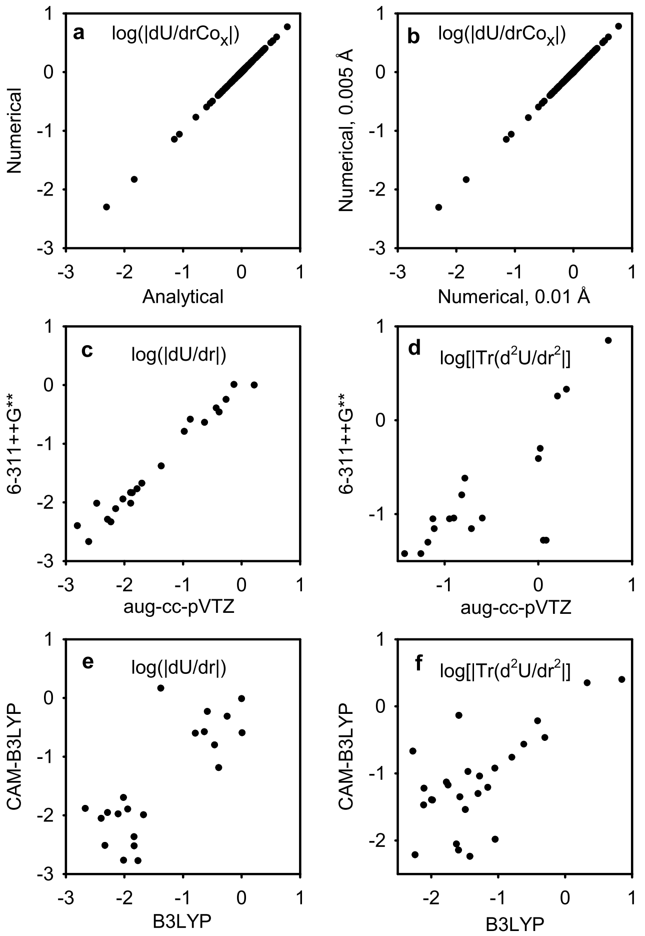

Figure 3. Diamine MO derivatives calculated at different levels: (a) Numerical vs analytical $\tilde{U}^a_{n,b}$ values, (b) numerical $\tilde{U}^a_{n,b}$ with different steps, (c, d) first and second derivatives ($\tilde{U}^a_{n,b}$ and $\tilde{U}^a_{nn,b}$) with two basis sets, and (e, f) first and second derivatives with two functionals, 6-311+G** basis set. (a, b) MOs 43−63 were included, for the x-coordinate of the Co atom, (c−f) highest occupied molecular orbital (HOMO) ± 3 included, gradient norm $|\mathrm{d}U/\mathrm{d}r| = (\tilde{U}_x^2 + \tilde{U}_y^2 + \tilde{U}_z^2)^{1/2}$ and second derivative trace $Tr(\mathrm{d}^2U/\mathrm{d}r^2) = (\tilde{U}_{xx} + \tilde{U}_{yy} + \tilde{U}_{zz})/3$, for the Co atom, and (a−d) B3LYP functional was used.

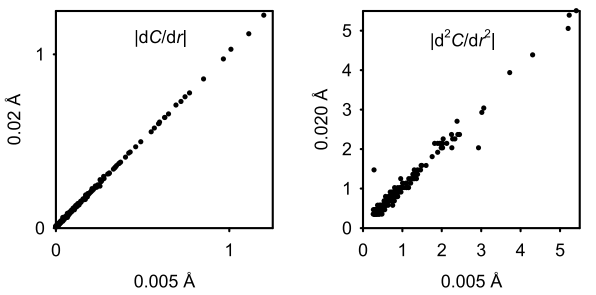

Figure 4. First and second CI coefficient derivatives (Co atom, x-coordinate, HOMO ± 10 excitations) as dependent (top, B3LYP/6-31G**) on the differentiation step.

Table 1. Basis Set and Functional Dependence of a CI Coefficient Derivative[a]

	B3LYP	B3PW91	CAM-B3LYP
6-31G*	0.3331	0.3221	0.3011
6-31G**	0.3354	0.3243	0.3065
6-311+G**	0.3392	0.3240	0.2823
6-311++G**	0.3409	0.3249	[b]
Def2TZVP	0.3502	0.3347	0.3301
aug-cc-pVTZ	0.3557	0.3373	[c]

[a] $[(\partial C/\partial x)^2 + (\partial C/\partial y)^2 + (\partial C/\partial z)^2]^{1/2}$, for the first excited electronic state, 50 → 53(β-MO) excitation and the Co atom. [b] SCF not converged. [c] Change in the orbital numbering.

be reasonably robust and accurate. The basis set and functional dependence are shown in Table 1. The coefficient was chosen as the largest one in the 50 → 53(β-MO) expansion so that the derivatives could be determined with good precision. The largest basis sets (Def2TZVP and aug-cc-pVTZ) provide about 5% larger values than the smaller ones. Similarly, the derivative (gradient norm) changes by 3−16% among the B3LYP, B3PW91, and CAM-B3LYP functionals.

These differences enter the perturbation terms responsible for the BBO corrections where they cause larger changes. This can be seen in Table 2 for a selected off-diagonal Hamiltonian element or in Figures S2 and S3 with the resultant spectra. To conclude these tests, we see that the DFT methodology provides a reasonably stable platform to estimate the BBO terms; however, a detailed basis set and functional dependence must be evaluated in the same way as for any other quantum-chemical computation.

Table 2. Functional and Basis Set Dependence of a Hamiltonian Interaction Element[a]

	B3LYP	B3PW91	CAM-B3LYP
6-31G*	1.024	1.102	0.848
6-31G**	0.951	0.807	0.703
6-311+G**	0.391	0.393	0.039
6-311++G**	0.297	0.341	[b]
Def2TZVP	0.338	0.339	0.388
aug-CC-pVTZ	0.912	0.133	1.152

[a] $\langle \nu_{kK}|V_{KJ}|\nu_{jJ}\rangle$ in cm^{-1}, $k = 32$ (CH and NH bending vibration), $K = 0$ (ground state), $J = 1$, $j = 0$. [b] SCF not converged.

4.4. Orbital BBO Contributions. Orbitals close to the highest occupied molecular orbital (HOMO)/lowest unoccupied molecular orbital (LUMO) pair contribute most to the effect because of their close energies and large overlaps. Core electrons are not much affected by changes in molecular geometry, and the contribution of high-energy virtual orbitals to states with low electronic energies quickly diminishes. The possibility to restrict the orbital range makes computations of the BBO terms faster. The numerical computation of the diffuse virtual orbital derivatives would also require tight SCF convergence criteria and laborious checks of similar orbitals in different differentiated geometries. For the diamine (53 α and 50 β electrons), the BBO VCD spectra in the CH stretching region were computed with HOMO ± 10, ± 20, and ± 30 orbitals included (Figure 5). The spectrum below 3000 cm^{-1} was virtually unaffected by the BBO correction. The CH stretching bands within ~3025 to 3150 cm^{-1} close to the first 3292 cm^{-1} electronic transition (electronic energies are listed in Table S1) exhibit minor intensity changes. The VCD shape with HOMO ± 20 still somewhat differs from that with HOMO ± 10, but the HOMO ± 20 and HOMO ± 30 curves are almost indistinguishable.

4.5. Large-Molecule Applications. The BO and BBO absorption and VCD spectra simulated for the sparteine−Co

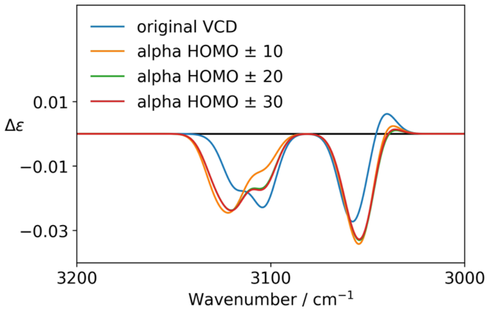

Figure 5. Diamine VCD spectra simulated within the BO approximation and the BBO results with HOMO ± 10−30 MOs included, at the B3LYP/6-31G** level.

and salicyl−Co complexes are compared to the experimental results in Figure 6. An encouraging agreement with the experimental behavior appears. Clearly, the absorption spectra simulated at the BO level are not much changed by the correction and correspond to the observations. Also, previous BO models on these and other systems provided a good agreement with experimental absorption intensities.[6,10] This is given by the small magnitude of the BBO energy terms/Hamiltonian matrix elements (e.g., Table 2) and consecutive very limited mixing of the electronic and vibrational BO states.

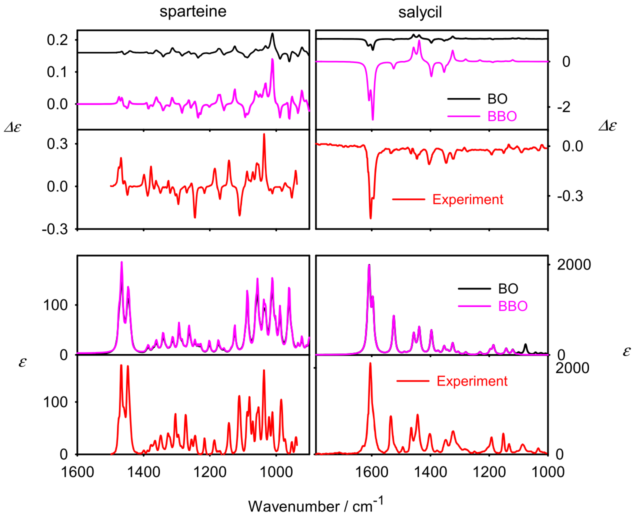

Figure 6. VCD (top) and absorption (bottom) spectra simulated for the sparteine−Co and salicyl−Co complexes within the BO and BBO approaches. The calculated harmonic frequencies were scaled to enhance the comparison of corresponding bands; the experiments are taken from refs 6 and 10.

On the other hand, the BBO correction causes significant changes in the VCD spectra. Some bands are enhanced up to 10 times. This dramatic difference of behavior of IR and VCD is explicable by the large magnetic moments and rotational strengths of the electronic transitions involving the d electrons. Indeed, in Table 3, we can see that the typical vibrational and electronic dipole strengths determining the absorption intensities are roughly comparable. Limited mixing of the electronic and vibrational states, therefore, cannot have an observable effect. On the other hand, rotational strengths of the first two electronic transitions (3.0056×10^{-4} and -1.6795×10^{-4} debyes^2) are relatively big, and even small contamination of the vibrational state by an electronic one results in a visible change of VCD intensity. A similar situation occurs for salicyl−Co (Table S3).

Table 3. Selected Sparteine−Co Transition Energies *E*, Dipole *D* and Rotational *R* Strengths, and the Kuhn Anisotropy (Dissymmetry) Factors $g = 4R/D$

E (cm^{-1})	$D \times 10^4$ (debye^2)	$R \times 10^8$ (debye^2)	$g \times 10^4$
	Vibrational		
1519	40	3	0.3
1514	33	−4	−0.5
1510	96	18	0.8
1505	5	−13	−9.3
1501	10	−9	−3.5
	Electronic		
5377	86	30 056	1403
5857	42	−16 795	−1588
8013	73	−8382	−459
11 520	3514	9903	11
12 257	3139	−7050	−9

The BBO correction makes the simulations closer to the experimental data, although for sparteine−Co the simulated intensities are smaller and for salicyl−Co they are bigger than observed (cf. the absolute *y*-scales). For salicyl−Co, the wrong sign of the signal around 1400 cm^{-1} is obtained. This can be explained not only by the approximations made during the BBO treatment but also by a high molecular flexibility, conformer equilibria,[10] and environmental factors, analysis of which goes beyond the scope of the present work. In particular, higher-order BBO corrections may be needed for a better agreement, which is not currently possible with our computational means. Nevertheless, we believe that already the first-order BBO corrections show their usefulness for interpretation of VCD spectra of transition-metal complexes and BBO phenomena in general.

5. CONCLUSIONS

Within the time-dependent density functional theory and simplified wave function model, we have elaborated on the expressions needed to correct IR and VCD intensities for electronic−vibrational interactions going beyond the Born−Oppenheimer approximation. Working expressions could be obtained, including overlap integrals between perturbed Slater determinants. The implementation was tested on a smaller molecule where it was found reasonably accurate and stable with respect to detailed parameters, such as the basis set and functional type. For two larger cobalt complexes, the BBO correction provided significant improvement of computed VCD intensities, although further tests are still needed in the future. In particular, the dependence on the basis set, environment, and inclusion of various BBO terms (e.g., first and second orbital/CI coefficient derivatives) could be explored only partially so far. In the present stage, many band signs and relative intensities differed in the simulated and experimental spectra. However, the computation provided a good theoretical basis for interpretation of the measured data. A large magnetic moment associated with the electronic transitions involving d electrons of the metal was identified as the key factor for the VCD enhancement. We believe that the possibility to reliably estimate the BBO coupling will significantly enhance the application span of VCD spectroscopy, including metal−ligand probes with the enhanced signal.

■ ASSOCIATED CONTENT

Supporting Information

The Supporting Information is available free of charge at https://pubs.acs.org/doi/10.1021/acs.jctc.0c00081.

> Non-BO matrix elements with perturbed electronic wave functions (Appendix I); developing the V_{KJ} elements for Slater/KS wave function (Appendix II); overlap integrals of Slater determinant derivatives (Appendix III); molecular orbital derivatives (Appendix IV); derivatives of the CI coefficients (Appendix V); electronic transition energies of the diamine (Table S1); sparteine−Co, Salycil−Co, and computational details (Table S2); selected salicyl−Co transition energies E, dipole D and rotational R strengths, and dissymmetry factors; diamine frontier molecular orbitals (Figure S1) (PDF)

■ AUTHOR INFORMATION

Corresponding Author

Petr Bouř − *Institute of Organic Chemistry and Biochemistry, Academy of Sciences, 16610 Prague, Czech Republic;* orcid.org/0000-0001-8469-1686; Email: bour@uochb.cas.cz

Author

Josef Tomeček − *Department of Chemistry, Imperial College London, London SW7 2AZ, United Kingdom*

Complete contact information is available at: https://pubs.acs.org/10.1021/acs.jctc.0c00081

Notes

The authors declare no competing financial interest.

■ ACKNOWLEDGMENTS

The work was supported by the Grant Agency of the Czech Republic (18-05770S (J.T.) and 20-10144S (P.B.)). We thank J. Cheeseman (Gaussian, Inc.) for the help with the Gaussian computations.

■ REFERENCES

(1) Born, M.; Oppenheimer, R. Zur Quantentheorie der Molekeln. *Ann. Phys.* **1927**, *389*, 457−284.

(2) Szabo, A.; Ostlund, N. S. *Modern Quantum Chemistry: Introduction to Advanced Electronic Structure Theory*; Dover: New York, 1989.

(3) Nafie, L. A. Theory of Vibrational Circular Dichroism and Infrared Absorption: Extension to Molecules with Low-Lying Excited Electronic States. *J. Phys. Chem. A* **2004**, *108*, 7222−7231.

(4) Keiderling, T. A.; Kubelka, J.; Hilario, J. Vibrational Circular Dichroism of Biopolymers. Summary of Methods and Applications. In *Vibrational Spectroscopy of Polymers and Biological Systems*; Braiman, M.; Gregoriou, V., Eds.; CRC Press: Boca Raton, 2006; pp 253−324.

(5) Nafie, L. *Vibrational Optical Activity: Principles and Applications*; Wiley: Chichester, 2011.

(6) He, Y.; Cao, X.; Nafie, L. A.; Freedman, T. B. Ab Initio VCD Calculation of a Transition-Metal Containing Molecule and a New Intensity Enhancement Mechanism for VCD. *J. Am. Chem. Soc.* **2001**, *123*, 11320−11321.

(7) Barnett, C. J.; Drake, A. F.; Kuroda, R.; Mason, S. F.; Savage, S. Vibrational-electronic interaction in the infrared circular dichroism spectra of transition-metal complexes. *Chem. Phys. Lett.* **1980**, *70*, 8−10.

(8) Johannessen, C.; Thulstrup, P. W. Vibrational circular dichroism spectroscopy of a spin-triplet bis-(biuretato) cobaltate(III) coordination compound with low-lying electronic transitions. *Dalton Trans.* **2007**, 1028−1033.

(9) Pescitelli, G.; Ludeke, S.; Chamayou, A. C.; Marolt, M.; Justus, V.; Gorecki, M.; Arrico, L.; Di Bari, L.; Islam, M. A.; Gruber, I.; Enamullah, M.; Janiak, C. Broad-Range Spectral Analysis for Chiral Metal Coordination Compounds: (Chiro)optical Superspectrum of Cobalt(II) Complexes. *Inorg. Chem.* **2018**, *57*, 13397−13408.

(10) Pescitelli, G.; Ludeke, S.; Gorecki, M.; Di Bari, L. Symmetry-Dependent Vibrational Circular Dichroism Enhancement in Co(II) Salicylaldiminato Complexes. *J. Phys. Chem. Lett.* **2019**, *10*, 650−654.

(11) Domingos, S. R.; Huerta-Viga, A.; Baij, L.; Amirjalayer, S.; Dunnebier, D. A.; Walters, A. J.; Finger, M.; Nafie, L. A.; de Bruin, B.; Buma, W. J.; Woutersen, S. Amplified vibrational circular dichroism as a probe of local biomolecular structure. *J. Am. Chem. Soc.* **2014**, *136*, 3530−3535.

(12) Stephens, P. J. Theory of Vibrational Circular Dichroism. *J. Phys. Chem. A.* **1985**, *89*, 748−752.

(13) Nafie, L. A. Velocity-gauge formalism in the theory of vibrational circular dichroism and infrared absorption. *J. Chem. Phys.* **1992**, *96*, 5687−5702.

(14) Yang, D.; Rauk, A. J. Vibrational circular dichroism intensities. Ab initio vibronic coupling theory using the distributed origin gauge. *J. Chem. Phys.* **1992**, *97*, 6517−6534.

(15) Nafie, L. A.; Freedman, T. B. Vibronic coupling theory of infrared vibrational transitions. *J. Chem. Phys.* **1983**, *78*, 7108−7116.

(16) Kohn, W.; Sham, L. J. Self-consistent equations including exchange and correlation effects. *Phys. Rev.* **1965**, *140*, A1133−A1138.

(17) Atkins, P. W.; Friedman, R. S. *Molecular Quantum Mechanics*, 3rd ed.; Oxford University Press:'New York, 1997.

(18) Barron, L. D. *Molecular Light Scattering and Optical Activity*; Cambridge University Press: Cambridge, UK, 2004.

(19) Sutcliffe, B. T.; Woolley, R. G. Comment on 'Molecular structure in non-Born−Oppenheimer quantum mechanics'. *Chem. Phys. Lett.* **2005**, *408*, 445−447.

(20) Guan, J.; Duffy, P.; Carter, J. T.; Chong, D. P.; Casida, K. C.; Casida, M. E.; Wrinn, M. Comparison of local-density and Hartree-Fock calculations of molecular polarizabilities and hyperpolarizabilities. *J. Chem. Phys.* **1993**, *98*, 4753−4765.

(21) Lipkowitz, K. B.; Cundari, T. R.; Elliot, P.; Furche, F.; Burke, K. Excited States from Time-dependent Density Functional Theory. In *Reviews in Computational Chemistry*; Lipkowitz, K. B.; Cundari, T. R., Eds.; John Wiley & Sons: Hoboken, New Jersey, 2009; Vol. *26*, pp 91−165.

(22) Štěpánek, P.; Bouř, P. Origin-Independent Sum Over States Simulations of Magnetic and Electronic Circular Dichroism Spectra via the Localized Orbital/Local Origin Method. *J. Comput. Chem.* **2015**, *36*, 723−730.

(23) Saxe, P.; Lengsfield, B. H.; Yarkony, D. R. On the evaluation of non-adiabatic coupling matrix elements for large scale CI wavefunctions. *Chem. Phys. Lett.* **1985**, *113*, 159−164.

(24) Barone, V.; Bloino, J.; Biczysko, M.; Santoro, F. Fully integrated approach to compute vibrationally resolved optical spectra: From small molecules to macrosystems. *J. Chem. Theory Comput.* **2009**, *5*, 540−554.

(25) Wilson, E. B.; Decius, J. C.; Cross, P. C. *Molecular Vibrations*; Dover: New York, 1980.

(26) Frisch, M. J.; Trucks, G. W.; Schlegel, H. B.; Scuseria, G. E.; Robb, M. A.; Cheeseman, J. R.; Scalmani, G.; Barone, V.; Petersson, G. A.; Nakatsuji, H.; Li, X.; Caricato, M.; Marenich, A. V.; Bloino, J.; Janesko, B. G.; Gomperts, R.; Mennucci, B.; Hratchian, H. P.; Ortiz, J. V.; Izmaylov, A. F.; Sonnenberg, J. L.; Williams; Ding, F.; Lipparini, F.; Egidi, F.; Goings, J.; Peng, B.; Petrone, A.; Henderson, T.; Ranasinghe, D.; Zakrzewski, V. G.; Gao, J.; Rega, N.; Zheng, G.; Liang, W.; Hada, M.; Ehara, M.; Toyota, K.; Fukuda, R.; Hasegawa, J.; Ishida, M.; Nakajima, T.; Honda, Y.; Kitao, O.; Nakai, H.; Vreven, T.; Throssell, K.; Montgomery, J. A., Jr.; Peralta, J. E.; Ogliaro, F.; Bearpark, M. J.; Heyd, J. J.; Brothers, E. N.; Kudin, K. N.; Staroverov, V. N.; Keith, T. A.; Kobayashi, R.; Normand, J.; Raghavachari, K.; Rendell, A. P.; Burant, J. C.; Iyengar, S. S.; Tomasi, J.; Cossi, M.;

Millam, J. M.; Klene, M.; Adamo, C.; Cammi, R.; Ochterski, J. W.; Martin, R. L.; Morokuma, K.; Farkas, O.; Foresman, J. B.; Fox, D. J. *Gaussian 16*, revision A.03; Wallingford, CT, 2016.

(27) Becke, A. D. A new mixing of Hartree−Fock and local density-functional theories. *J. Chem. Phys.* **1993**, *98*, 1372−1377.

(28) Klamt, A.; Schuurmann, G. COSMO: A New Approach to Dielectric Screening in Solvent with Explicit Expression for the Screening Energy and its Gradient. *J. Chem. Soc., Perkin Trans. 2* **1993**, 799−805.

(29) Cossi, M.; Barone, V. Analytical second derivatives of the free energy in solution by polarizable continuum models. *J. Chem. Phys.* **1998**, *109*, 6246−6254.

(30) Caricato, M.; Ingrosso, F.; Mennucci, B.; Tomasi, J. A time-dependent polarizable continuum model: Theory and application. *J. Chem. Phys.* **2005**, *122*, No. 154501.

(31) Duboc, C.; Gennari, M. Experimental Techniques for Determining Spin States. In *Spin States in Biochemistry and Inorganic Chemistry: Influence on Structure and Reactivity*; Swart, M.; Costas, M., Eds.; Willey: Chichester, 2016; pp 59−83.

(32) Mason, S. F.; Peacock, R. D. Complexes of some first-row transition elements with (-)-spartein. *J. Chem. Soc., Dalton Trans.* **1973**, *2*, 226−228.

(33) Pople, J. A.; Krishnan, R.; Schlegel, H. B.; Binkley, J. S. Derivative studies in Hartree-Fock and Møller-Plesset Theories. *Int. J. Quantum Chem.* **1979**, *13*, 225−241.

(34) Johnson, B. G.; Frisch, M. J. An implementation of analytic second derivatives of the gradient-corrected density functional energy. *J. Chem. Phys.* **1994**, *100*, 7429−7442.

https://dx.doi.org/10.1021/acs.jctc.0c00081
J. Chem. Theory Comput. 2020, 16, 2627−2634